Quasiparticle states around a nonmagnetic impurity in electron-doped iron-based superconductors with spin-density-wave order

Tao Zhou, Huaixiang Huang, Yi Gao, Jian-Xin Zhu, and C. S. Ting

Phys. Rev. B **83**, 214502 — Published 1 June 2011

DOI: 10.1103/PhysRevB.83.214502

Quasiparticle states around a nonmagnetic impurity in electron-doped iron-based superconductors with spin-density-wave order

Tao Zhou,[1,2] Huaixiang Huang,[1,3] Yi Gao,[1] Jian-Xin Zhu,[4] and C. S. Ting[1]
[1]*Texas Center for Superconductivity and Department of Physics, University of Houston, Houston, Texas 77204, USA*
[2]*Department of Physics, Nanjing University of Aeronautics and Astronautics, Nanjing 210016, China*
[3]*Department of Physics, Shanghai University, shanghai 200444, China*
[4]*Theoretical Division, Los Alamos National Laboratory, Los Alamos, New Mexico 87545, USA*
(Dated: May 3, 2011)

The quasiparticle states around a nonmagnetic impurity in electron-doped iron-based superconductors with spin-density-wave (SDW) order are investigated as a function of doping and impurity scattering strength. In the undoped sample, where a pure SDW state exists, two impurity-induced resonance peaks are observed around the impurity site and they are shifted to higher (lower) energies as the strength of the positive (negative) scattering potential (SP) is increased. For the doped samples where the SDW order and the superconducting order coexist, the main feature is the existence of sharp in-gap resonance peaks whose positions and intensity depend on the strength of the SP and the doping concentration. In all cases, the local density of states exhibits clear C_2 symmetry. We also note that in the doped cases, the impurity will divide the system into two sublattices with distinct values of magnetic order. Here we use the band structure of a two-orbital model, which considers the asymmetry of the As atoms above and below the Fe-Fe plane. This model is suitable to study the properties of the surface layers in the iron-pnictides and should be more appropriate to describe the scanning tunneling microscopy experiments.

PACS numbers: 74.70.Xa, 74.55.+v

I. INTRODUCTION

The new family of iron-based superconducting (SC) materials has attracted much attention since their discovery.[1] The parent compounds exhibit a spin-density-wave (SDW) order at low temperatures. Upon doping either electrons or holes into the system, the SDW order is suppressed and superconductivity emerges, suggesting the interplay and competition between these two states.

The impurity effect is an important property in the studies of superconductivity. One prominent feature of *d*-wave paring symmetry in cuprates is the existence of bound states near the impurity, which is revealed by both experiments and theoretical calculations.[2] For iron-based superconducting materials, the impurity effect in the SC state has also been theoretically studied intensively.[3–10] It was proposed that a single nonmagnetic impurity could be used to distinguish the pairing symmetry and the in-gap bound states could exist for the typical $s_\pm$ pairing symmetry.[8–10] The in-gap bound states for $s_\pm$ pairing should be different from those in cuprates due to the absence of quasiparticle excitations at low energy. On the other hand, in the SDW state, it was proposed experimentally that the Fermi surface (FS) is only partially gapped and small ungapped Fermi pockets exist at low temperature.[11–16] This feature was recently reproduced based on a two-orbital model together with a mean-field approach.[17] The gap-like feature and the existence of tiny ungapped regions along the diagonal direction of the Brillouin zone (BZ) are quite similar to the case of the *d*-wave SC gap in cuprates. Therefore, one would expect that the low-energy bound states should also exist in the SDW state for the iron-based materials. So far, the impurity effect in the SDW state remains less explored and a systematic study of this problem is still lacking. We believe it is timely and quite interesting to address this issue theoretically and verify the aforementioned expectation numerically. Furthermore, in some of the iron-based materials the SC and SDW orders are proposed to coexist in the underdoped regime.[18–26] The issue is still a subject of discussion and we anticipate that the impurity effect could provide additional signatures for the coexistence of these two orders.

In this paper, we study theoretically the impurity effect on a two-dimensional square lattice based on a two-orbital model and the Bogoliubov-de Gennes (BdG) equations. By introducing a single impurity into the system, the local density of states (LDOS) is calculated and our results show that: (i) In the undoped sample, there are two impurity-induced resonance peaks at and near the impurity site and the LDOS spectra exhibit C_2 symmetry, with one-dimensional modulation. (ii) The impurity effect in various doped cases is also studied. Its effect on the LDOS is remarkable only when the strength of the scattering potential (SP) is larger than a certain value. For weak and moderate SPs, a distinct bound state exists explicitly at the next-nearest-neighbor (nnn) sites of the impurity, the energy of which depends on the strength and sign of the SP, as well as on the doping concentration. For the unitary impurity, there is a sharp in-gap peak at low doping; while at high doping, the impurity induced bound state is close to the SC coherence peaks. On the other hand, in a small range of moderate doping there are two in-gap peaks only for positive SP. All the above features could be used to detect the presence of the SDW order as well as the coexistence of the SDW and SC orders.

The paper is organized as follows. In Sec. II, we introduce the model and work out the formalism. In Sec. III, we study the FS. In Sec. IV, the impurity effect in the parent compound is investigated. In Secs. V and VI, we study the impurity effect in doped regime for positive and negative SPs, respectively. Finally, we give a summary in Sec. VII.

II. MODEL AND FORMALISM

The iron-based superconducting materials have a layered structure with the FeAs layers being the superconducting planes. In the present work, following Refs. [9] and [17], we start from a two-orbital model with on-site interaction. Here the two orbitals are d_{xz} and d_{yz} orbitals of Fe ions. The As ions are above and below the Fe-Fe plane alternatively. Since the next-nearest-neighbor hoppings are mediated by As ions. The hopping through the up As ions does not equal to that through down As ions. This asymmetry should be correct when one investigates the surface properties because the bonds between up As ions and Fe ions are broken when cleavage. Previously based on this model, the theoretical results are qualitatively consistent with both the ARPES[27] and STM[28] experiments. For example, based on this model, the obtained phase diagram,[17] spin susceptibility,[29] as well as the Andreev bound state inside the vortex core[30] are all consistent with the experiments. Thus we also use it to investigate the impurity effect. The Hamiltonian is written as,

$$H = H_{BCS} + H_{int} + H_{imp} \ . \tag{1}$$

Here H_{BCS} is the BCS-like Hamiltonian, which includes the hopping term and the pairing term, expressed by,

$$\begin{aligned} H_{BCS} \ = \ & -\textstyle\sum_{\mathbf{i}\mu\mathbf{j}\nu\sigma}(t_{\mathbf{i}\mu\mathbf{j}\nu}c^{\dagger}_{\mathbf{i}\mu\sigma}c_{\mathbf{j}\nu\sigma}+h.c.)-t_0\sum_{\mathbf{i}\mu\sigma}c^{\dagger}_{\mathbf{i}\mu\sigma}c_{\mathbf{i}\mu\sigma} \\ & +\textstyle\sum_{\mathbf{i}\mu\mathbf{j}\nu\sigma}(\Delta_{\mathbf{i}\mu\mathbf{j}\nu}c^{\dagger}_{\mathbf{i}\mu\sigma}c^{\dagger}_{\mathbf{j}\nu\bar{\sigma}}+h.c.) \ , \end{aligned} \tag{2}$$

where $\mathbf{i} = (i_x, i_y)$, $\mathbf{j} = (j_x, j_y)$ are the site indices, $\mu, \nu = 1, 2$ are the orbital indices, and t_0 is the chemical potential. H_{int} is the on-site interaction term. At the mean-field level, it can be written as:[17,31,32]

$$\begin{aligned} H_{int} = \ & U\sum_{\mathbf{i}\mu\sigma\neq\bar{\sigma}}\langle n_{\mathbf{i}\mu\bar{\sigma}}\rangle n_{\mathbf{i}\mu\sigma}+U'\sum_{\mathbf{i},\mu\neq\nu,\sigma\neq\bar{\sigma}}\langle n_{\mathbf{i}\mu\bar{\sigma}}\rangle n_{\mathbf{i}\nu\sigma} \\ & +(U'-J_H)\sum_{\mathbf{i},\mu\neq\nu,\sigma}\langle n_{\mathbf{i}\mu\sigma}\rangle n_{\mathbf{i}\nu\sigma} \ , \end{aligned} \tag{3}$$

where $n_{\mathbf{i}\mu\sigma}$ is the density operator at site $\mathbf{i}$ and orbital μ, with spin σ. The quantity U' is taken to be $U-2J_H$.[32] The impurity part of the Hamiltonian, H_{imp}, is given by:

$$H_{imp} = \sum_{\mathbf{i_m}\mu\sigma} V_s c^{\dagger}_{\mathbf{i_m}\mu\sigma}c_{\mathbf{i_m}\mu\sigma} \ . \tag{4}$$

Here the impurity means that the Fe ion is replaced by a different atom. Thus the on-site energy of the ion is changed and acts as the scattering center. Thus in the present work, following Refs. [9,10,17], we here consider only the intra-orbital scattering by a nonmagnetic impurity.

The mean-field Hamiltonian (1) can be diagonalized by solving the BdG equations self-consistently,

$$\sum_{\mathbf{j}}\sum_{\nu}\begin{pmatrix} H_{\mathbf{i}\mu\mathbf{j}\nu\sigma} & \Delta_{\mathbf{i}\mu\mathbf{j}\nu} \\ \Delta^{*}_{\mathbf{i}\mu\mathbf{j}\nu} & -H^{*}_{\mathbf{i}\mu\mathbf{j}\nu\bar{\sigma}}\end{pmatrix}\begin{pmatrix} u^{n}_{\mathbf{j}\nu\sigma} \\ v^{n}_{\mathbf{j}\nu\bar{\sigma}}\end{pmatrix} = E_n\begin{pmatrix} u^{n}_{\mathbf{i}\mu\sigma} \\ v^{n}_{\mathbf{i}\mu\bar{\sigma}}\end{pmatrix}, \tag{5}$$

with

$$\begin{aligned} H_{\mathbf{i}\mu\mathbf{j}\nu\sigma} = \ & -t_{\mathbf{i}\mu\mathbf{j}\nu}+[U\langle n_{\mathbf{i}\mu\bar{\sigma}}\rangle+(U-2J_H)\langle n_{\mathbf{i}\bar{\mu}\bar{\sigma}}\rangle \\ & +(U-3J_H)\langle n_{\mathbf{i}\bar{\mu}\sigma}\rangle+v_s\delta_{\mathbf{i},\mathbf{i_m}}-t_0]\delta_{\mathbf{ij}}\delta_{\mu\nu} \ , \end{aligned} \tag{6}$$

and

$$\Delta_{\mathbf{i}\mu\mathbf{j}\nu} = \frac{V_{\mathbf{i}\mu\mathbf{j}\nu}}{4}\sum_{n}(u^{n}_{\mathbf{i}\mu\uparrow}v^{n*}_{\mathbf{j}\nu\downarrow}+u^{n}_{\mathbf{j}\nu\uparrow}v^{n*}_{\mathbf{i}\mu\downarrow})\tanh(\frac{E_n}{2K_BT}) \ , \tag{7}$$

$$\langle n_{\mathbf{i}\mu}\rangle \ = \ \sum_{n}|u^{n}_{\mathbf{i}\mu\uparrow}|^2 f(E_n)+\sum_{n}|v^{n}_{\mathbf{i}\mu\downarrow}|^2[1-f(E_n)] \ . \tag{8}$$

Here $V_{\mathbf{i}\mu\mathbf{j}\nu}$ is the pairing strength and $f(x)$ is the Fermi-Dirac distribution function. The SC order parameter at site $\mathbf{i}$ is defined as

$$\Delta_i = \frac{\Delta_{i,i+\hat{x}+\hat{y}}+\Delta_{i,i-\hat{x}-\hat{y}}+\Delta_{i,i+\hat{x}-\hat{y}}+\Delta_{i,i-\hat{x}+\hat{y}}}{4} \ , \tag{9}$$

in accordance with the $s_{\pm}$ pairing symmetry.

The LDOS is calculated according to

$$\rho_{\mathbf{i}}(\omega) = \sum_{n\mu}[|u^{n}_{\mathbf{i}\mu\sigma}|^2\delta(E_n-\omega)+|v^{n}_{\mathbf{i}\mu\bar{\sigma}}|^2\delta(E_n+\omega)] \ , \tag{10}$$

where the delta function $\delta(x)$ is taken as $\Gamma/\pi(x^2+\Gamma^2)$, with the quasiparticle damping $\Gamma = 0.01$.

Following Ref. [9], we use the hopping constants,

$$t_{\mathbf{i}\mu,\mathbf{i}\pm\hat{\alpha}\mu} \ = \ t_1 \qquad (\alpha = \hat{x}, \hat{y}) \ , \tag{11}$$

$$t_{\mathbf{i}\mu,\mathbf{i}\pm(\hat{x}+\hat{y})\mu} \ = \ \frac{1+(-1)^{\mathbf{i}}}{2}t_2+\frac{1-(-1)^{\mathbf{i}}}{2}t_3 \ , \tag{12}$$

$$t_{\mathbf{i}\mu,\mathbf{i}\pm(\hat{x}-\hat{y})\mu} \ = \ \frac{1+(-1)^{\mathbf{i}}}{2}t_3+\frac{1-(-1)^{\mathbf{i}}}{2}t_2 \ , \tag{13}$$

$$t_{i\mu,\mathbf{i}\pm\hat{x}\pm\hat{y}\nu} \ = \ t_4 \qquad (\mu \neq \nu) \ . \tag{14}$$

In the present work, we use $t_{1-4} = 1, 0.4, -2, 0.04$.[9] t_0 is determined by the electron filling per site n ($n = 2 + x$). The on-site Coulombic interaction U and Hund's coupling J_H are taken as 3.4 and 1.3, respectively. The pairing is chosen as nnn intra-orbital pairing with the pairing strength $V = 1.2$. This kind of pairing is consistent with the $s_{\pm}$-pairing[33–37] and has been widely used in previous theoretical studies based on the BdG technique.[8,17,31] The numerical calculation is performed on a 32×32 square lattice with the periodic boundary conditions. A 30×30 supercell is taken to calculate the LDOS. Throughout the paper, the energy and length are measured in units of t_1 and the Fe-Fe distance a, respectively. The temperature is set to be $T = 0$. In the following, all the results we presented have been checked by using different initial values and they remain qualitatively the same, suggesting the reliability of our calculation.

III. FERMI SURFACE TOPOLOGY IN THE SDW STATE

The impurity effect is expected to have an intimate relation with the FS topology. As a result, the impurity effect in the SDW state is model dependent. In order to investigate the impurity effect in the iron-based superconductors with SDW order, firstly we need to study the FS in the SDW state.

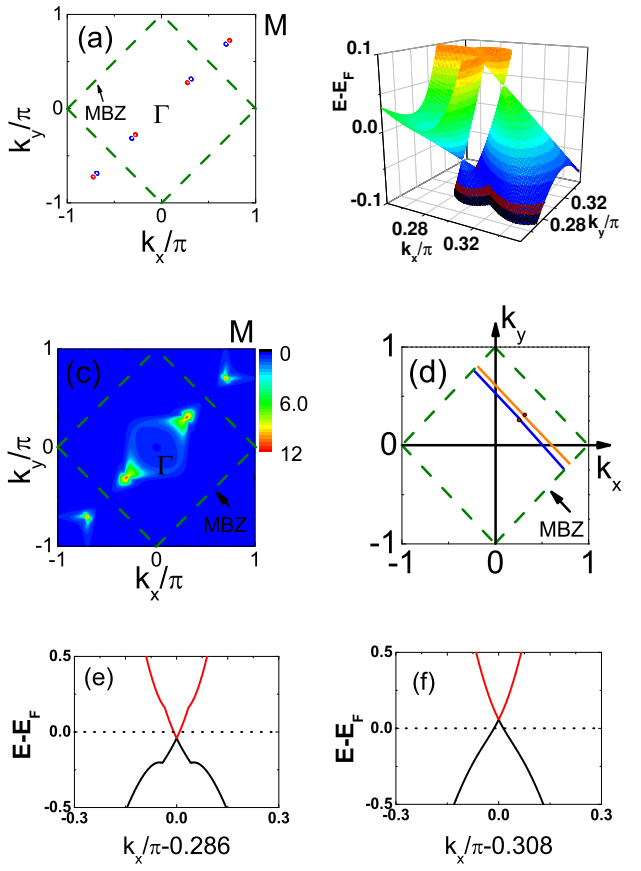

FIG. 1: (Color online) (a) The zero temperature SDW FS. (b) Two Dirac cones at $(k_x, k_y) = (0.286\pi, 0.286\pi)$ and $(k_x, k_y) = (0.308\pi, 0.308\pi)$, respectively. (c) The spectral function $A(\mathbf{k}, \omega)$ integrated from $\omega = -0.1$ to $\omega = 0.1$. (e) and (f) are the band structures near the Fermi energy along the blue [goes through $(k_x, k_y) = (0.286\pi, 0.286\pi)$] and orange [goes through $(k_x, k_y) = (0.308\pi, 0.308\pi)$] lines in (d), respectively. The BZ is defined in the 2Fe/cell representation and the green dashed line in (a), (c) and (d) represents the MBZ.

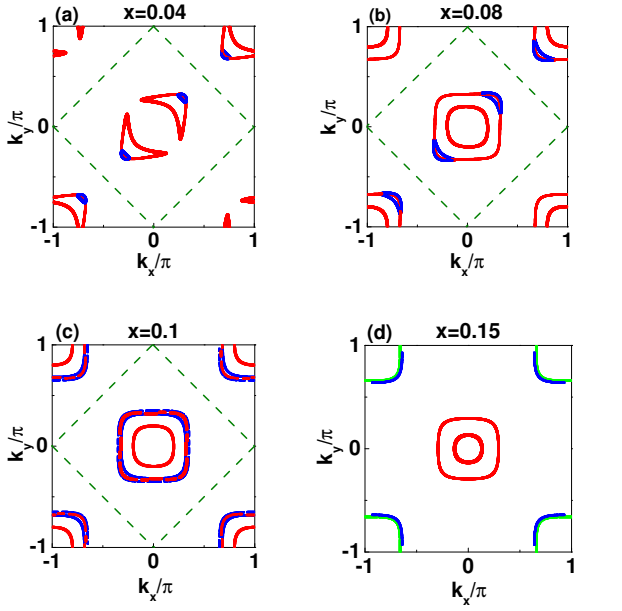

FIG. 2: (Color online) The zero temperature SDW FS at various doping levels. The SC order Δ is artificially set to zero in order to illustrate the effect of SDW on the evolution of the FS. The blue and red pockets in the $x = 0.04$, 0.08 and 0.1 cases are both electron pockets. The green dashed line is the same as that in Fig. 1

At zero doping, below the SDW temperature, it was proposed experimentally that there exist small FSs along the Γ-M line of the BZ and Dirac cones in the electronic structure form inside these FSs, with their apices being located close to the Fermi energy. However, whether these FSs and Dirac cones are electron- or hole-like is within uncertainties of the experiment.[11] On the other hand, theoretically it was shown that in both a two-band model and a five-band model, nodes in the SDW gap function must exist due to the symmetry-enforced degeneracy at the Γ and M high-symmetry points, even in the presence of perfect nesting, but the number and locations of these nodes are model dependant.[38] Therefore, whether they correspond to the experimentally observed Dirac cones is still unclear. In Fig. 1, we plot the zero temperature SDW FS and the corresponding band structure near the Fermi energy obtained by our self-consistent calculation. As we can see from Fig. 1(a), in the SDW state, there remain four small FS pockets in the magnetic Brillouin zone (MBZ), two of which are electron-like (red) located around $(k_x, k_y) = \pm(0.286\pi, 0.286\pi)$, while the other two are hole-like (blue) located around $(k_x, k_y) = \pm(0.308\pi, 0.308\pi)$. The pockets outside the MBZ are just replica of those inside it due to band-folding in the SDW state and they can be connected by the SDW wave vector $\mathbf{Q} = (\pi, \pi)$. The areas enclosed by these pockets are equal, thus keeping the doping level at $x = 0$. Inside these four pockets, there are four Dirac cones. As shown in Fig. 1(b), the apex of the Dirac cone is 0.026 below the Fermi energy at $(k_x, k_y) = \pm(0.286\pi, 0.286\pi)$ while it is 0.046 above the Fermi energy at $(k_x, k_y) = \pm(0.308\pi, 0.308\pi)$, suggesting that they are electron- and hole-like Dirac cones, respectively. The spectral function $A(\mathbf{k}, \omega)$, which is proportional to the photoemission intensity measured in ARPES experiments, is integrated from $\omega = -0.1$ to $\omega = 0.1$ and shown in Fig. 1(c). As we can see, the locations of the bright spots are around $(k_x, k_y) = \pm(0.3\pi, 0.3\pi)$ and the equivalent symmetry points outside the MBZ, on the Γ-M line, in qualitative agreement with experiment.[11] In addition, although most parts of the original FSs around Γ are gapped by the SDW order, the gap value is extremely small on these FSs. Thus, around Γ, the low-energy spectral function has moderate intensity and this can be seen from the ring structure around Γ with lower intensity, as compared to those bright spots. We also notice that the system has only two-fold symmetry when entering the SDW state while the experimentally observed four-fold symmetry is due to the superposition of twin domains or domain averaging, as suggested in Refs. 11 and 12, respectively. The band structures near the Fermi energy

scanned along the blue and orange cuts in Fig. 1(d) are plotted in Figs. 1(e) and 1(f), respectively. It clearly shows the X-like structure of Dirac cones and again suggests that the Dirac cone is electron-like at $(k_x, k_y) = (0.286\pi, 0.286\pi)$ and hole-like at $(k_x, k_y) = (0.308\pi, 0.308\pi)$. The locations of the FS pockets and the bright spots in the spectral function are consistent with the experimental observation, but in our calculation, the electron- and hole-like Dirac cones appear in-pairs and are located very close to each other along the Γ-M line of the BZ, the apices of which are both in the vicinity of the Fermi energy, thus we propose this to be directly verified by future ARPES experiments with higher resolution. In addition, the existence of electron and hole Dirac cone states in-pairs has already been confirmed indirectly by measuring the magnetoresistance.[39]

Figure 2 shows the evolution of the FS with doping. Here, we set the SC order Δ to zero to illustrate the effect of SDW on the evolution of the FS. In the MBZ, as doping increases, the size of the electron pockets [the red pockets shown in Fig. 1(a)] is enlarged while that of the hole pockets [the blue pockets shown in Fig. 1(a)] is reduced. When doping increases to about $x = 0.02$, the hole pockets vanish completely. By further increasing doping, another two electron pockets appear in the MBZ [the blue pockets in the $x = 0.04, 0.08$ and 0.1 cases shown in Fig. 2], exactly at the same locations where the hole pockets vanish and overlap with the original electron pockets. The size of all these electron pockets is enlarged with doping. If we define the areas enclosed by the inner and outer red lines to be S_1 and those enclosed between the inner and outer blue lines to be S_2, then we have $x = 2N_xN_y(S_1 + S_2)$, with N_x, N_y being the linear dimensions of the square lattice. Finally, when $x = 0.15$, the SDW order disappears and there is no more band-folding due to it. In this case, there are two electron pockets and two hole pockets around the M and Γ points of the BZ, respectively.

IV. IMPURITY SCATTERING EFFECT IN UNDOPED SAMPLE

Based on a toy model and phenomenological calculation,[40] it was proposed that the impurity induced bound state should appear near the impurity site for the undoped sample. However, the actual band structure and FS should be important for the features of the order parameters and LDOS. Thus we will reexamine this issue based on the two-orbital model and present a detailed investigation of the nonmagnetic impurity effect in the parent compound. Here we consider both positive and negative impurity SPs. A single impurity is put at site (16, 16). We define the on-site magnetic order parameter, $M_{\mathbf{i}} = (-1)^{i_x}\frac{1}{4}\sum_{\mu}(n_{\mathbf{i}\mu\uparrow} - n_{\mathbf{i}\mu\downarrow})$. This definition is suitable for the typical $(\pi, 0)$ SDW order, consistent with previous experiments[41] and theoretical calculations.[17,31]

The intensity plots of the site-dependent particle number $n_i = \sum_{\mu}(n_{i\mu\uparrow} + n_{i\mu\downarrow})$ and magnetic order M_i in real space are shown in Fig. 3. The left panels of Fig. 3 plot the spatial distribution of the particle number. For positive SP, electrons are repelled by the impurity, therefore at the impurity site the value of particle number is reduced. Increasing the positive SP will lead to smaller values of n_i at the impurity site, which, when $V_s > 6$, will vanish. For negative SP, on the contrary, electrons are attracted to the impurity and larger $|V_s|$ will lead to a higher particle number at the impurity site. The particle numbers will recover to the bulk value 2.0 at about 2 lattice constants away from the impurity site for both positive and negative SPs. In doped samples, these characteristics of n_i do not change except that the value of n_i far away from the impurity site will be $2 + x$, where x is the electron doping concentration.

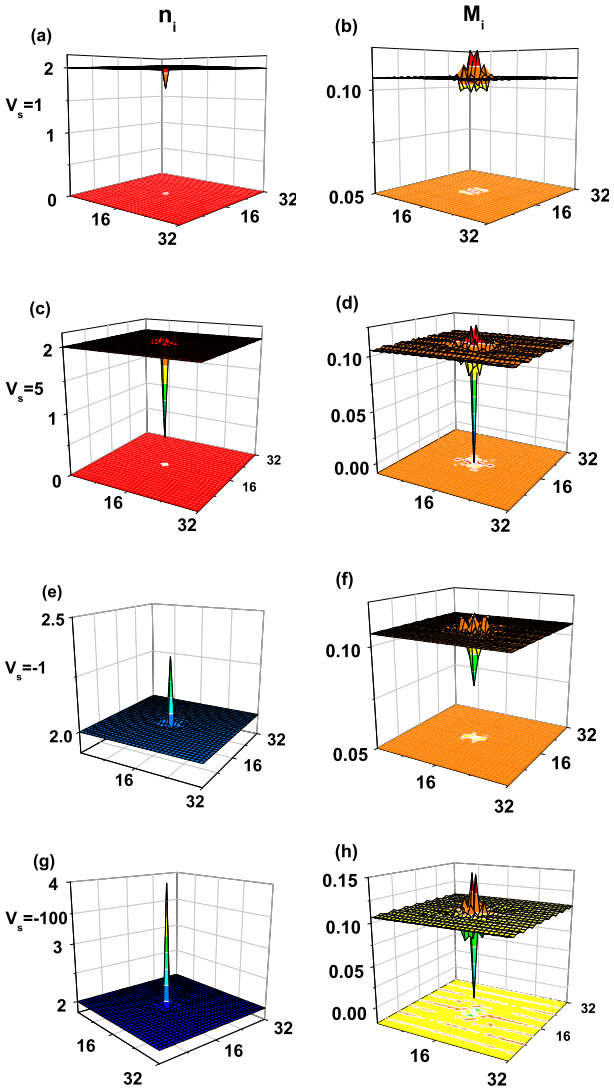

FIG. 3: (Color online) The intensity plots of the particle number (left panels) and magnetic order (right panels) at zero doping and zero temperature for different SPs $V_s = 1, 5, -1, -100$.

The right panels of Fig. 3 show the real space modulation of the magnetic order M_i. For small positive SP $V_s = 1$, the values of magnetic order oscillate near the impurity site with the maximum $M_i = 0.115$ at the impurity site, slightly higher than the bulk value 0.105. For moderate SP $V_s = 5$, the magnitude

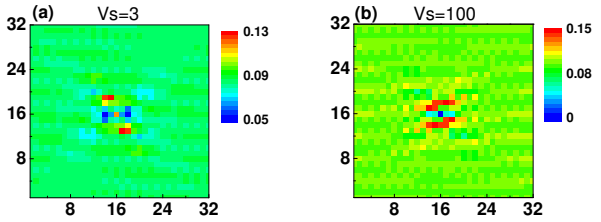

FIG. 4: (Color online) The intensity plots of the LDOS at zero energy for different SPs $V_s = 3$ and $V_s = 100$.

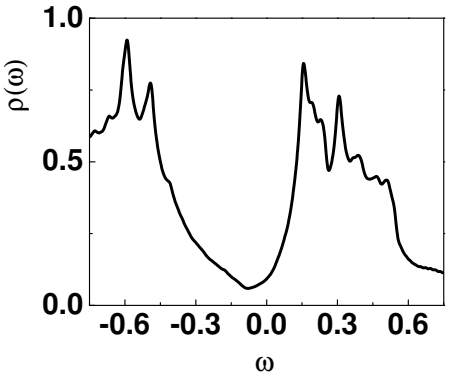

FIG. 5: The bulk LDOS in the SDW state of undoped sample.

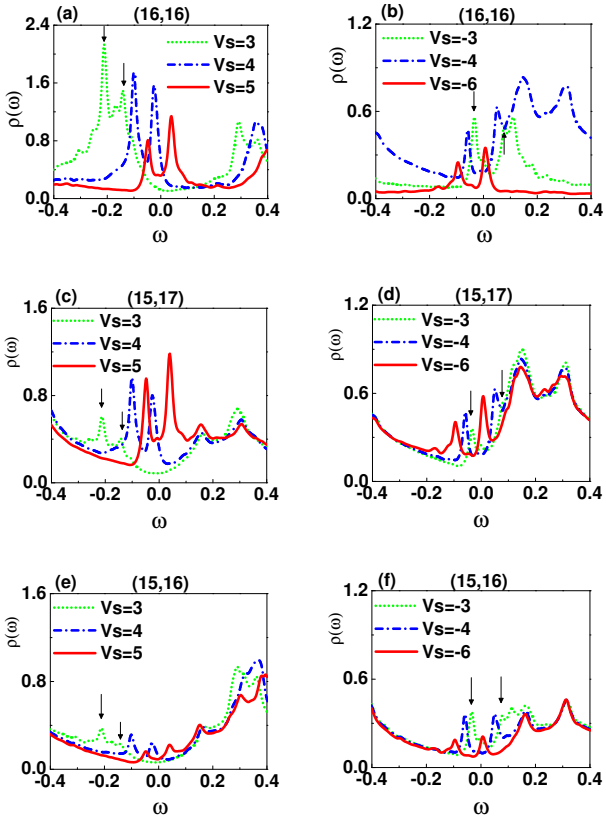

FIG. 6: (Color online) (a) The LDOS at the impurity site as a function of ω, for different positive SPs $V_s = 3, 4, 5$. (b) is similar to (a), but for negative SPs $V_S = -3, -4, -6$. (c) and (d) [(e) and (f)] are similar to (a) and (b), respectively, but are plotted at site $(15, 17)$ [$(15, 16)$].

of M_i drops down almost to zero at the impurity site, with the maximum $M_i \sim 0.12$ appearing in the vicinity of the impurity site. We thus expect that stronger SP will lead to stronger oscillation of M_i around the impurity and this is verified by setting $V_s = \pm 100$, for which we take $V_s = -100$ as an example as shown in Fig. 3. From the corresponding plot we can see that the modulation of M_i is very strong around the impurity, similar to Friedel oscillation and it will recover to the impurity-free value at about $4 \backsim 5$ lattice constants away from the impurity site. Order parameters for negative SP $V_s = -1$ are also shown, unlike the enhanced M_i in the $V_s = 1$ case, we find that the magnitude of M_i is suppressed at the impurity site and the oscillation of M_i is stronger than the $V_s = 1$ case.

We now study the low-energy impurity-induced bound states. The intensity plots of the LDOS in real space at zero energy are shown in Fig. 4 for $V_s = 3$ and $V_s = 100$, respectively. As seen, for $V_s = 3$ the LDOS at the impurity site $(16, 16)$ is finite while for nearly unitary SP $V_s = 100$ it vanishes. The LDOS modulates near the impurity site and some bright spots can be seen clearly around the impurity, indicating the existence of bound states at low energy. Another prominent feature revealed from the LDOS map in Fig. 4 is the four-fold symmetry breaking which is more obvious near the impurity. The symmetry of the system reduces to C_2 and it survives for various SPs no matter whether they are positive or negative. Furthermore, there also exists one-dimensional modulation of the LDOS along the y-axis even when it is far away from the impurity. This feature is similar to the experimentally observed nematic electronic structure,[42] thus supporting the impurity effect as a possible candidate for the formation of nematic order. As the bias deviates from zero, the nematic order still exists and it survives in the case of multiple impurities. Since in the two-orbital model we use, each unit cell contains two inequivalent Fe atoms, the existence of an impurity on either site of the unit cell will naturally break the four-fold symmetry of the system, thus we conclude that the breaking of the four-fold symmetry in the LDOS is induced not only by the SDW order, but also by the intrinsic asymmetry pinned by the impurity.

We proceed to study the energy and site dependence of the LDOS. Without impurity, the LDOS is uniform and site independent, with its minimum located at negative energy, consistent with STM experiment.[28] There are two coherence peaks at negative energies and two at positive energies, as shown in Fig. 5. Since the LDOS has finite value at the impurity site for weak SP, we plot it exactly at the impurity site for both positive and negative SPs in Fig. 6. For positive impurity potential $V_s = 3$ the spectrum displays two distinct resonance peaks at negative energies which are denoted by two arrows. The intensity of the left peak is higher than that of the right one. The

splitting of the resonance peaks is due to the presence of the inter-orbital coupling t_4 and the resonance peaks are related to the opening of SDW gap. As V_s is increased the two resonance peaks shift to higher energies and the intensities of the peaks decrease as shown in Fig. 6(a). At last, the intensity of the right peak becomes higher than that of the left one. For $V_s = 6$, the LDOS at the impurity site nearly vanishes. The feature of the LDOS for negative SPs shown in Fig. 6(b) is different from that in the positive SP case, for example, the intensities of the peaks are much lower. For $V_s = -3$, double peaks show up at both sides of the Fermi energy, which we also denote by two arrows. These peaks shift to lower energies with increased value of $|V_s|$. As V_s reaches to $V_s = -8$, the LDOS at the impurity site also vanishes.

In Figs. 6(c) and 6(d) we plot the LDOS at nnn site $(15, 17)$ of the impurity for positive and negative SPs, respectively. One can see that with increased strength of SP, the double peaks move to higher (lower) energies for positive (negative) SP. For positive SP, increasing impurity strength will lead to increased peak intensities and this is in contrast to that at the impurity site. However, for negative SP, the situation is similar to that at the impurity site. Figures 6(e) and 6(f) plot the LDOS at nn site $(15, 16)$. It is shown that the intensities of the impurity-induced resonance peaks are much lower than those at the impurity site $(16, 16)$, although the characteristics are similar. Since the impurity has four nnn and nn sites, and the system has only C_2 symmetry, there are two inequivalent nnn and nn sites, respectively. The LDOS at the other nnn site $(15, 15)$ and nn site $(16, 15)$ does not show the impurity-induced resonance peaks at low energies (not shown here) and resembles the bulk LDOS, again suggesting the four-fold symmetry breaking.

The properties of the low-energy bound states shown in Fig. 6 are significantly different from those in the pure SC state.[9,10,17] In the pure SC state, the bound states would appear for the $s_{\pm}$ pairing symmetry. The existence of the resonance peaks is due to the scattering between the hole-pockets and electron-pockets. Because the pairing function changes sign thus the bound state appears due to the Andreev reflection. This effect has already been studied in Ref. 9 by using T-matrix method and in Ref. 43 based on a different two-orbital model by using T-matrix and BdG methods. In the pure SDW state, the bound state is coming from the quasipaticles in Dirac cones, similar to the resonance state near an impurity in graphene.[44] The energies of the bound states are close to the Fermi energy so that they can be easily detected by experiments. Therefore, we expect that the results presented in this work can also be used as an effective method to justify the ARPES experiment.

V. POSITIVE IMPURITY SCATTERING IN DOPED SAMPLES

As we have discussed above, in both pure SDW state and pure SC state, the bound states are induced by a single non-magnetic impurity. Since the detailed features of the resonance peaks are quite different between these two cases, the impurity effect in the underdoped regime where the SC and SDW orders coexist is an intriguing question. In particular, both theoretical analyses[17] and experimental observations[18–26] do suggest the coexistence of these two orders in this regime. In the following, we will not plot the real space particle number since it is similar to the undoped case. We mention that around the moderate doping $x = 0.08$, the impurity could induce a weak charge density wave for various SPs. However, the $\delta n/(2 + x)$ is less than 0.5%, so we neglect it.

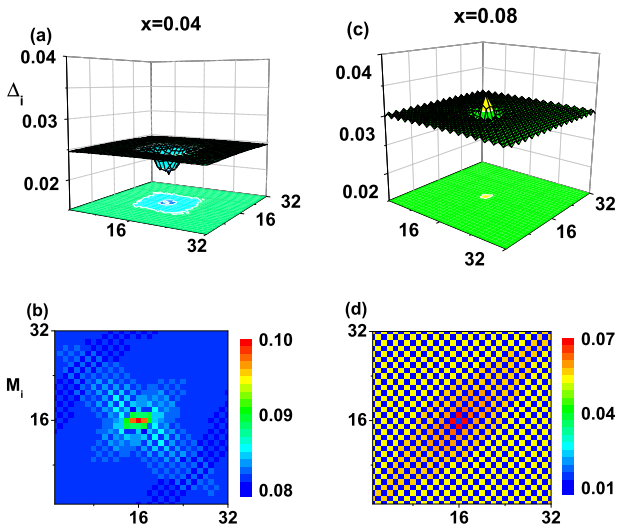

FIG. 7: (Color online) The intensity plots of the SC [(a) and (c)] and magnetic [(b) and (d)] orders for weak SP $V_s = 1$, at doping $x = 0.04$ and $x = 0.08$, respectively.

For small SP $V_s = 1$, we can see from Fig. 7(a) that at low doping $x = 0.04$, the amplitude of the SC order Δ_i is reduced at and around the impurity site, which will recover to the impurity-free value at about 6 lattice constants away from the impurity. But the SC order is not always suppressed at the impurity site. As doping is increased to $x \geq 0.08$, at the impurity site the magnitude of the SC order is enhanced [see Fig. 7(c)], which means the impurity is not a pair breaker in this case. At $x = 0.04$, the magnetic order M_i at the impurity site is enhanced, similar to that in the undoped case and we notice that there exist modulations along the diagonal directions as can be seen from Fig. 7(b). At $x = 0.08$, the pattern of magnetic order changes, the system separates into two sublattices explicitly. The value of M_i in one sublattice is about 0.05, while in the other one is ~ 0.007, with $M_i \sim 0.01$ at the impurity site. This impurity-induced two-sublattice pattern of magnetic order survives until the doping level is beyond the region where the SDW and SC orders coexist. At higher doping $x = 0.12$, Δ_i is enhanced just like the $x = 0.08$ case, but with a vanishingly small value of M_i.

For larger SP $V_s = 3.0$, the order parameters are similar to those for $V_s = 1.0$, except that M_i is reduced at the impurity site at all doping levels. As doping increases to $x = 0.08$, the system also separates into two sublattices.

The LDOS has finite values at the impurity site for small SP

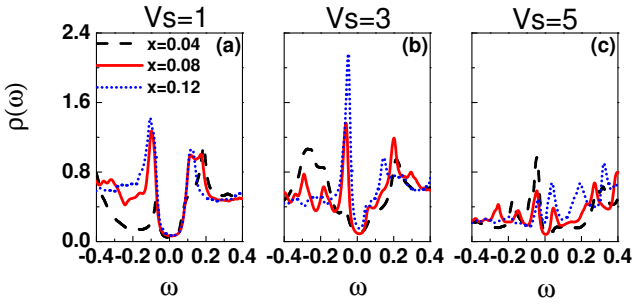

FIG. 8: (Color online) The LDOS at the impurity site as a function of ω for $V_s = 1, 3, 5$, at different doping levels $x = 0.04, 0.08, 0.12$.

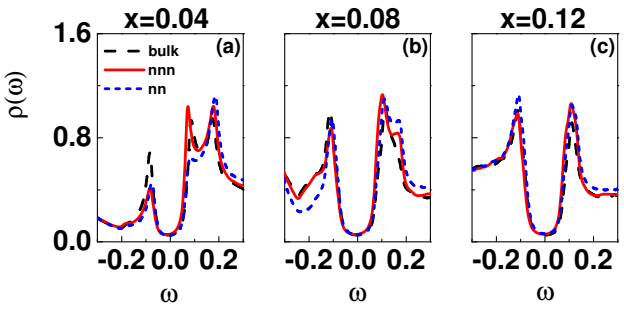

FIG. 9: (Color online) For $V_s = 1$, the LDOS on nn and nnn sites of the impurity as a function of ω at various doping levels. The black dashed line represents the bulk LDOS.

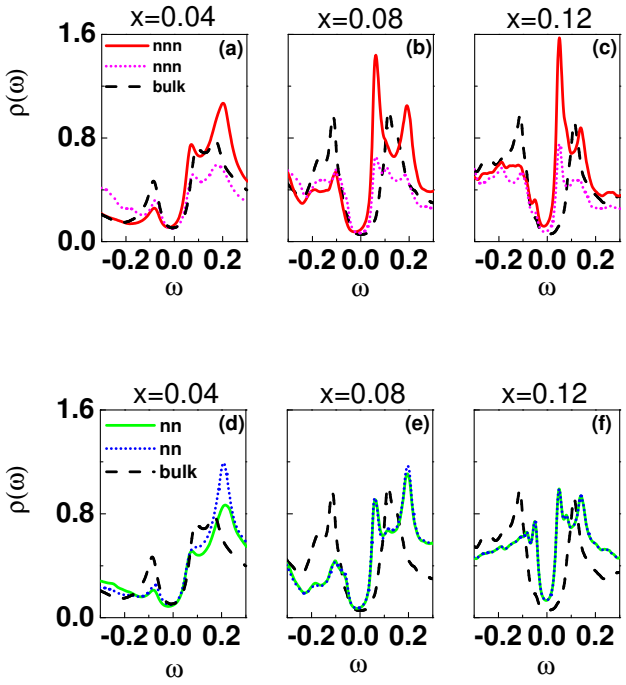

FIG. 10: (Color online) For $V_s = 3$, the LDOS on nn and nnn sites of the impurity as a function of ω at various doping levels. The upper panel is for the two nnn sites $(15, 15)$ (red solid) and $(15, 17)$ (pink short dot) and the lower one is for the two nn sites $(15, 16)$ (green solid) and $(16, 15)$ (blue short dot). The black dashed line represents the bulk LDOS.

in all doped samples, but unlike the undoped one, the double resonance peaks are absent. For $V_s = 1$, the effect of the impurity on the LDOS is shown in the left panel of Fig. 8. In this case, at $x = 0.04$, the intensities of the SC coherence peaks at both positive and negative energies are suppressed by the impurity. On the other hand, at doping $x \geq 0.08$, the negative SC coherence peak is enhanced by the impurity while the positive one remains almost unchanged. For larger SP $V_s = 3$, at $x = 0.04$, the intensities of the SC coherence peaks are further suppressed. When $x = 0.08$ there is a sharp in-gap resonance peak located at negative energy and close to the SC coherence peak [see Fig. 8(b)]. As doping is increased to $x = 0.12$, the intensity of the in-gap peak becomes higher. On the other hand, for moderate SP $V_s = 5$, at $x = 0.04$, there exists an in-gap bound state at negative energy while at both $x = 0.08$ and $x = 0.12$, there are two in-gap bound states, one at positive energy, the other one at negative energy. The magnitude of the LDOS at all doping levels becomes considerably smaller and reaches to zero for larger SP.

For $V_s = 1.0$, the impurity induces only minor modulations on the LDOS around the impurity site, which is similar to the bulk LDOS at all doping levels [see Fig. 9]. The positive energy peak at nn and nnn sites is higher than the negative one at low doping $x = 0.04$. As x increases, the intensity of the negative resonance peak gradually becomes higher than that of the positive one, similar to the evolution of the bulk LDOS with doping.[28] Although the system does not have C_4 symmetry, the main features of the LDOS at the four nnn (nn) sites are similar to each other, thus in Fig. 9, we only plot the LDOS at one of the nnn (nn) sites for clarity.

As the SP increases to $V_s = 3.0$, we show the LDOS at two inequivalent nnn (nn) sites in the upper (lower) panel of Fig. 10. At low doping $x = 0.04$, the effect of the impurity is weak and no in-gap bound states exist at nnn and nn sites. At a higher doping $x = 0.08$, a single in-gap resonance peak shows up at both the two nnn sites with different intensities, but their positions are similar to each other, both are located at positive energy and close to one of the SC coherence peaks. There is also a single in-gap peak at the two nn sites, the LDOS of which is identical to each other. As the doping increases to $x = 0.12$, the LDOS at the nnn sites is similar to the $x = 0.08$ case, except for a higher peak intensity at positive energy and the addition of a hump at negative energy on one of the nnn sites, which will evolve into a resonance peak when further increasing doping (not shown here). The LDOS at the two nn sites is also identical to each other and clearly shows two in-gap resonance peaks.

For moderate SP $V_s = 5$, the difference of the LDOS between the two inequivalent nnn sites $(15, 15)$ and $(15, 17)$ be-

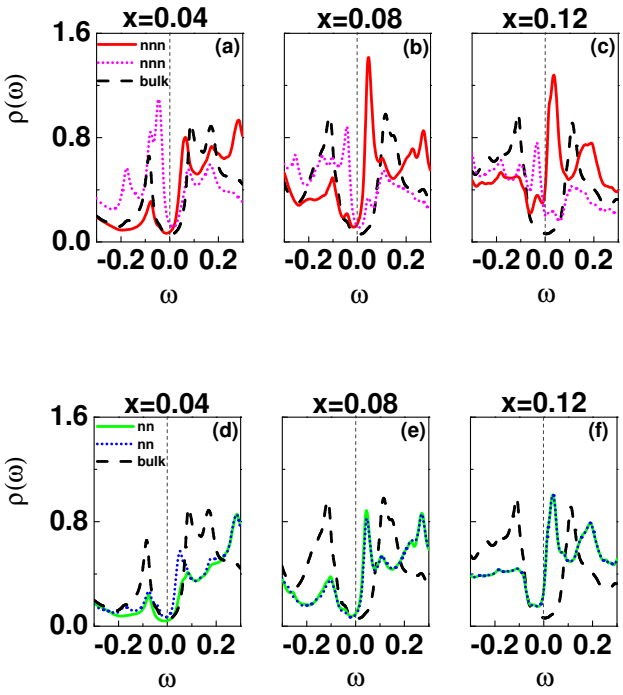

FIG. 11: (Color online) Similar to Fig. 10, bur for $V_s = 5$.

comes remarkable [see the upper panel of Fig. 11]. At one of the nnn sites the single in-gap resonance peak is located at positive energy while at the other one it is located at negative energy. As the doping increases, the peaks at the two nnn sites move closer to the Fermi energy. On the other hand, at the two nn sites $(15, 16)$ and $(16, 15)$, there is a single in-gap resonance peak located above the Fermi energy at all dopings. At low doping the LDOS spectra at the two nn site are different. As the doping increases the peaks shift to the Fermi energy and the LDOS at the two nn sites will become identical.

For nearly unitary positive SP $V_s = 100$, the SC and magnetic orders are both suppressed and oscillate in the vicinity of the impurity site and their magnitudes reach the minimum exactly at the impurity site. The suppressed order parameters recover to their bulk value at about 3 lattice constants away from the impurity. We note that when $x \geq 0.04$ the system will separate into two sublattices. The difference of M_i between the two sublattices is larger at $x = 0.08$ than that at $x = 0.04$ while the magnitude of M_i decreases with doping and will vanish at $x > 0.1$.

Since the LDOS at the impurity site is zero for such a strong SP, we thus plot it on nnn and nn sites of the impurity in Fig .13, at various dopings. At $x = 0.02$, a sharp in-gap resonance peak appears close to zero energy on the positive side. It shifts to negative energy with reduced intensity as x increases to 0.04. When $x \geq 0.05$ two in-gap resonance peaks show up. As the doping increases further, they are pushed away by each other and merge into the SC coherence peaks of the bulk LDOS at $x \geq 0.08$. In all cases, the LDOS exhibits clear C_2

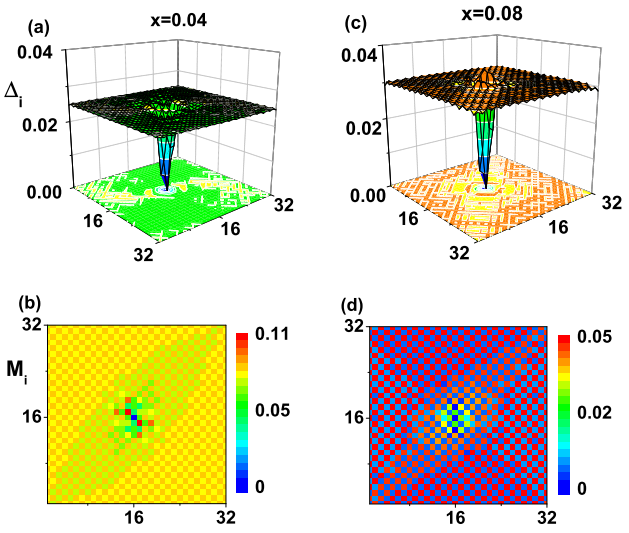

FIG. 12: (Color online) Similar to Fig. 7, but for $V_s = 100$.

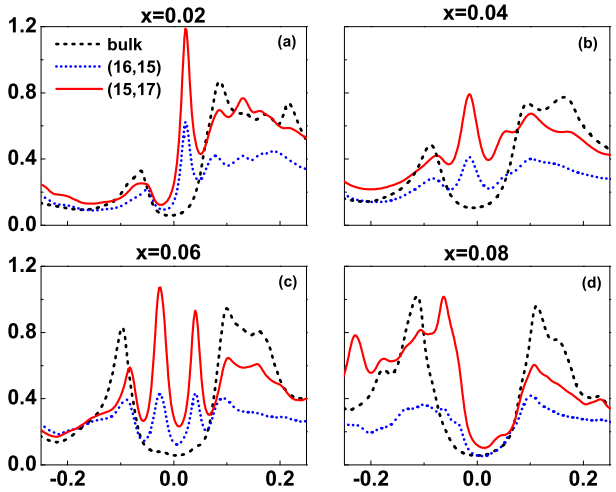

FIG. 13: (Color online) The LDOS on nn and nnn sites of the impurity as a function of ω, for $V_s = 100$. Different panels correspond to different doping levels. The red solid line denotes the nnn site $(15, 17)$ while the blue dashed line denotes the nn site $(16, 15)$, with the bulk LDOS denoted by the black dashed line.

symmetry. However, the LDOS on the inequivalent nn (nnn) sites is qualitatively the same, thus we choose the sites $(16, 15)$ and $(15, 17)$ as an example for convenience.

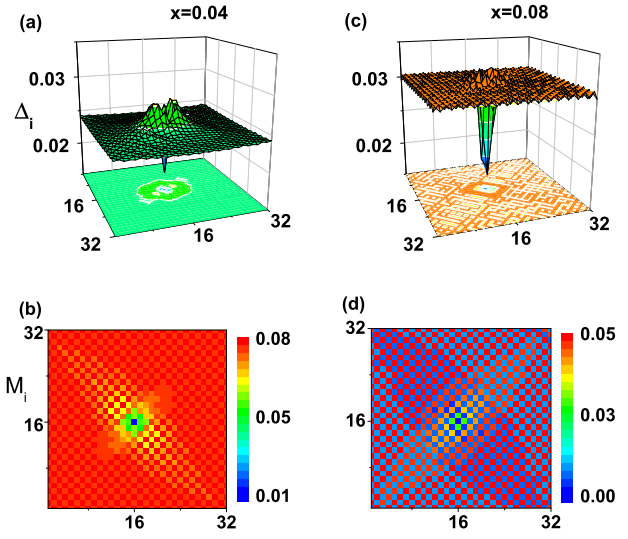

FIG. 14: (Color online) Similar to Fig. 7, but for $V_s = -3$.

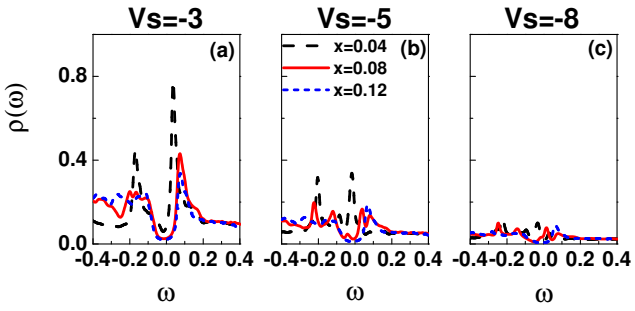

FIG. 15: (Color online) The LDOS at the impurity site as a function of ω at different dopings $x = 0.04, 0.08, 0.12$, for $V_s = -3, -5, -8$.

VI. NEGATIVE IMPURITY SCATTERING IN DOPED SAMPLES

In real materials, both positive and negative SPs are possible, and the response of the system to the impurity may depend on the sign of the SP, thus we discuss the negative SP case in this section.

As we can see from Fig. 14, for $V_s = -3$, the impurity induces oscillation of the SC order with Δ_i being suppressed at the impurity site and enhanced on several nearby sites at $x = 0.04$. At a higher doping $x = 0.08$, around the impurity site Δ_i is suppressed and the oscillation is not distinct. The magnitude of M_i is suppressed at the impurity site at all doping levels and apparently M_i will divide into two sublattices at ra elatively higher doping. At $x = 0.08$, at the impurity site M_i is close to zero, and is 0.05 and 0.01 on the two sublattices, respectively.

Being contrary to the $V_s = 3$ case where the impurity effect is stronger at a relatively higher doping, the in-gap resonance

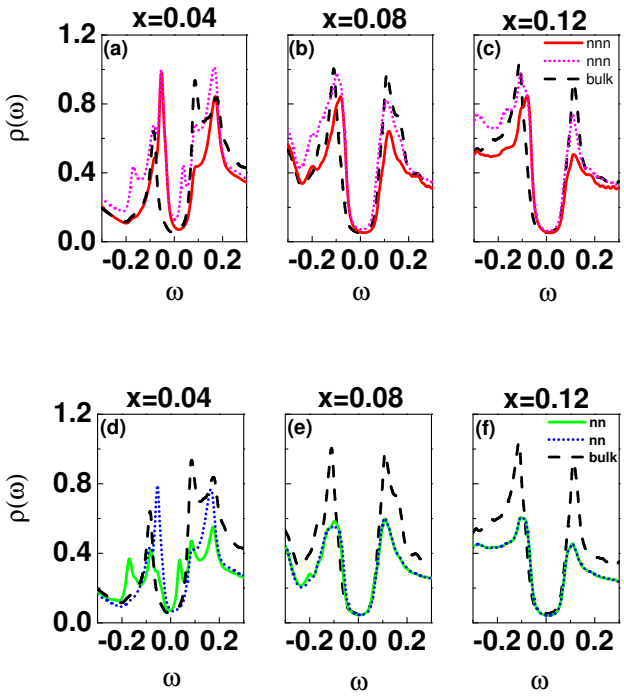

FIG. 16: (Color online) For $V_s = -3$, the LDOS on nnn and nn sites of the impurity as a function of ω at various dopings. The upper and lower panels are for nnn and nn sites, respectively. The bulk LDOS is denoted by the black dashed line.

peak for negative SP is clearer at a lower doping. From Fig. 15 we can see, for $V_s = -3$, at the impurity site there is a sharp in-gap resonance peak at positive energy at a low doping $x = 0.04$. At a higher doping, the LDOS at the impurity site has two peaks at the edge of the SC coherence peaks with the right peak being higher than the left one. Here we do not show the SC coherence peaks in Fig. 15, but in Figs. 16 and 18 we plot the corresponding bulk LDOS in which the SC coherence peaks are explicitly shown. As the SP strength increases to $V_s = -5$, the corresponding peaks are all suppressed and in the $x = 0.04$ case, the in-gap resonance peak shifts towards the Fermi energy. From the Fig. 15(b) we can see that the intensity of the LDOS at the impurity site nearly vanishes for $V_s = -8$.

We also plot the LDOS on nnn and nn sites for $V_s = -3$ in Fig. 16, at different dopings. At $x = 0.04$, the LDOS on both the nnn and nn sites shows the existence of in-gap resonance peaks, which gradually merge into the SC coherence peaks as the doping increases. Again, the breaking of four-fold symmetry is more obvious on the nnn sites than it is on the nn sites. As the doping increases, this asymmetry tends to diminish.

For strong negative potential $V_s = -8$, both the SC and magnetic orders are suppressed at the impurity site and oscillate around it [see Fig. 17]. At about 4 lattice constants away from the impurity, the SC and magnetic orders recover to their

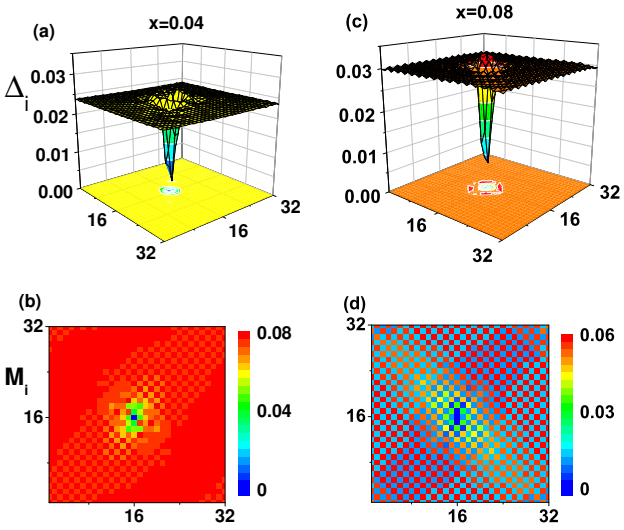

FIG. 17: (Color online) Similar to Fig. 7, but for $V_s = -8$.

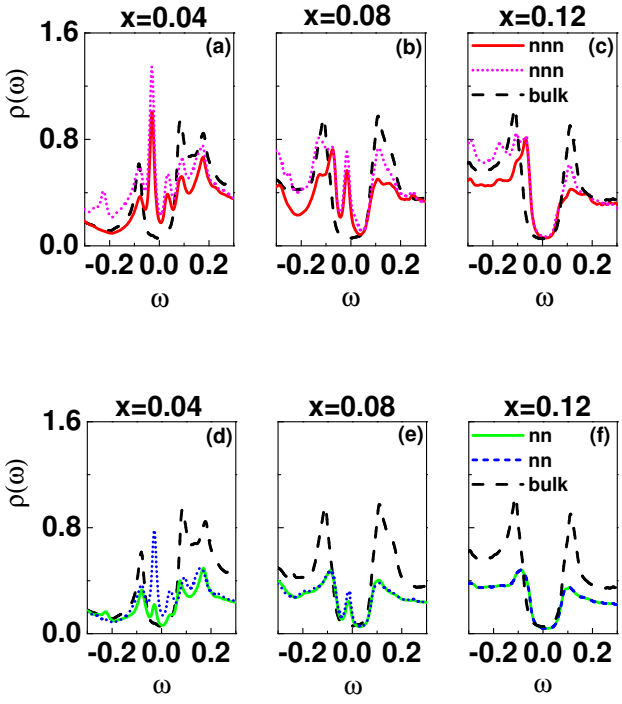

FIG. 18: (Color online) Similar to Fig. 16, but for $V_s = -8$.

bulk values. At doping $x = 0.08$, M_i also separates into two sublattices as can be seen from Fig. 17(d).

As shown in Fig. 18, there are in-gap resonance peaks on all the nnn and nn sites at $x = 0.04$. The breaking of the four-fold symmetry is minor, although still visible. The intensities of the in-gap peaks are suppressed with increased doping. At $x = 0.12$ the in-gap peaks are near the gap edge and merge into the coherent peaks. The profile of the LDOS on nn sites is similar to that on nnn sites, except that the corresponding peaks are lower and the asymmetry is weaker.

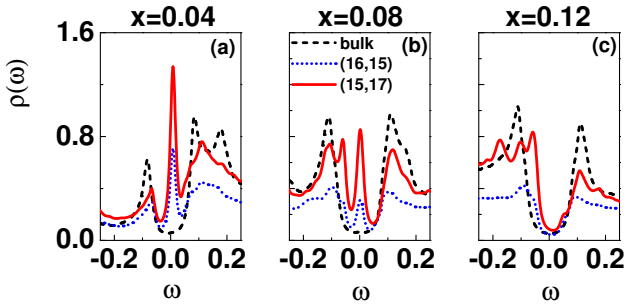

FIG. 19: (Color online) For $V_s = -100$, the LDOS on nnn and nn sites as a function of ω, at different dopings. The red solid and blue dotted lines denote the LDOS on nnn and nn sites, respectively. The black dashed line represents the bulk LDOS.

For a nearly unitary negative potential $V_s = -100$, the real space distributions of the SC and magnetic orders are similar to the positive unitary potential case. Fig. 19 shows the LDOS on nnn and nn sites at various dopings. Similar to the strong positive SP case, there is a sharp in-gap peak at a low doping $x = 0.04$, the position of which is almost at the Fermi energy. We believe that this sharp peak is due to the existence of the SDW order. As the doping increases to $x = 0.08$, the height of the in-gap peak drops and becomes lower than that of the SC coherence peak. As the doping increases to $x = 0.12$, the in-gap peaks are very close to the SC coherence peaks.

VII. SUMMARY

By solving the BdG equations self-consistently, it is shown that without impurity, at zero doping and in the SDW state, there exist equal-sized electron- and hole-like FS pockets along the Γ-M line of the BZ, inside which the Dirac cones form. The electron- and hole-like Dirac cones appear in-pairs near the Fermi energy and are located very close to each other. The effect of electron doping is mainly to reduce the size of the hole pockets while increase that of the electron ones, consistent with the increased electron density.

When impurity is introduced into the system, we find that in the parent compound, strong SP, being repulsive or attractive, could induce considerably large oscillation of the magnetic order around the impurity site. In addition, for all the SP strength we investigated, there exists one-dimensional modulation of the LDOS, similar to the experimentally observed nematic electronic structure, thus supporting the impurity effect as a possible candidate for the formation of nematic order. Furthermore, two impurity-induced resonance peaks are observed around the impurity site and they are shifted to higher (lower) energies as the strength of the positive (negative) SP is increased.

In doped samples, generally speaking, the SC and magnetic orders are suppressed at and around the impurity site, with more complicated variations compared to those in cuprates. However, for positive SP at higher doping or negative SP at lower doping, the SC order may even be enhanced at or around the impurity site, suggesting that the impurity is not a pair breaker in this case. In addition, impurity could separate the system into two sublattices denoted by two different values of magnetic order, which can be seen more clearly at relatively higher doping. Furthermore, there exist impurity-induced bound states at and around the impurity site, whose positions and intensities depend on the strength and sign of the SP, as well as on the doping concentration. For weak and moderate SPs, a distinct bound-state peak shows up explicitly in the LDOS at the nnn sites to the impurity. For a unitary impurity, there is a sharp in-gap peak at low doping, while at high doping, the impurity induced bound state is close to the SC coherence peaks. On the other hand, in a small range of moderate doping there are two in-gap peaks only for positive SP.

In all cases, the impurity breaks the four-fold symmetry of the system and has a stronger effect on nnn sites than it does on nn sites as can be seen from the LDOS. This symmetry breaking is induced not only by the SDW order, but also by the intrinsic asymmetry in our model pinned by the impurity. All the above features could be used to detect the presence of the SDW order and to probe the coexistence of the SDW and SC orders.

Acknowledgments

This work was supported by the Texas Center for Superconductivity at the University of Houston and by the Robert A. Welch Foundation under the Grant No. E-1146 (T.Z., H.H., and C.S.T.) and E-1070 (Y.G.), the NSFC under Grant No. 11004105 (T.Z.), the U.S. DOE at LANL under Contract No. DE-AC52-06NA25396, the U.S. DOE Office of Basic Energy Science, and the LANL LDRD Program (J.-X.Z.).

[1] Y. Kamihara, T. Watanabe, M. Hirano, and H. Hosono, J. Am. Chem. Soc. **130**, 3296 (2008).
[2] A. V. Balatsky, I. Vekhter, and Jian-Xin Zhu, Rev. Mod. Phys. **78**, 373 (2006).
[3] A. V. Chubukov, D. V. Efremov, and I. Eremin, Phys. Rev. B **78**, 134512 (2008).
[4] Y. Bang, H. Y. Choi, and H. Won, Phys. Rev. B **79**, 054529 (2009).
[5] D. Parker, O. V. Dolgov, M. M. Korshunov, A. A. Golubov, and I. I. Mazin, Phys. Rev. B **78**, 134524 (2008).
[6] Y. Senga and H Kontani, New J. Phys. **11**, 035005 (2009).
[7] A. B Vorontsov, M. G. Vavilov, and A. V. Chubukov, Phys. Rev. B **79**, 140507(R) (2009).
[8] Tao Zhou, Xiang Hu, Jian-Xin Zhu, and C. S. Ting, arxiv: 0904.4273.
[9] Degang Zhang, Phys. Rev. Lett. **103**, 186402 (2009).
[10] W. F. Tsai, Y. Y. Zhang, C. Fang, and J. P. Hu, Phys. Rev. B **80**, 064513 (2009).
[11] P. Richard, K. Nakayama, T. Sato, M. Neupane, Y.-M. Xu, J. H. Bowen, G. F. Chen, J. L. Luo, N. L. Wang, X. Dai, Z. Fang, H. Ding, and T. Takahashi, Phys. Rev. Lett. **104**, 137001 (2010).
[12] D. Hsieh, Y. Xia, L. Wray, D. Qian, K. Gomes, A. Yazdani, G.F. Chen, J.L. Luo, N.L. Wang, and M. Z. Hasan, arxiv: 0812.2289.
[13] S. de Jong, E. van Heumen, S. Thirupathaiah, R. Huisman, F. Massee, J. B. Goedkoop, R. Ovsyannikov, J. Fink, H. A. Duerr, A. Gloskovskii, H.S. Jeevan, P. Gegenwart, A. Erb, L. Patthey, M. Shi, R. Follath, A. Varykhalov, M. S. Golden, Europhys. Lett. **89**, 27007 (2010).
[14] M. Yi, D. H. Lu, J. G. Analytis, J.-H. Chu, S.-K. Mo, R.-H. He, M. Hashimoto, R. G. Moore, I. I. Mazin, D. J. Singh, Z. Hussain, I. R. Fisher, and Z.-X. Shen, Phys. Rev. B **80**, 174510 (2009).
[15] S. E. Sebastian, J. Gillett, N. Harrison, P. H. C. Lau, D. J. Singh, C. H. Mielke, and G. G. Lonzarich, J. Phys.: Condens. Matter **20**, 422203 (2008).
[16] J. G. Analytis, R. D. McDonald, J.-H. Chu, S. C. Riggs, A. F. Bangura, C. Kucharczyk, M. Johannes, and I. R. Fisher, Phys. Rev. B **80**, 064507 (2009).
[17] Tao Zhou, Degang Zhang, and C. S. Ting, Phys. Rev. B **81**, 052506 (2010).
[18] D. K. Pratt, W. Tian, A. Kreyssig, J. L. Zarestky, S. Nandi, N. Ni, S. L. Budko, P. C. Canfield, A. I. Goldman, and R. J. McQueeney, Phys. Rev. Lett. **103**, 087001 (2009).
[19] X. F. Wang, T. Wu, G. Wu, R. H. Liu, H. Chen, Y. L. Xie, and X. H. Chen, New J. Phys. **11**, 045003 (2009).
[20] Y. Laplace, J. Bobroff, F. Rullier-Albenque, D. Colson, and A. Forget, Phys. Rev. B **80**, 140501(R) (2009).
[21] C. Lester, J. -H. Chu, J. G. Analytis, S. C. Capelli, A. S. Erickson, C. L. Condron, M. F. Toney, I. R. Fisher, and S. M. Hayden, Phys. Rev. B **79**, 144523 (2009).
[22] A. D. Christianson, M. D. Lumsden, S. E. Nagler, G. J. MacDougall, M. A. McGuire, A. S. Sefat, R. Jin, B. C. Sales, and D. Mandrus, Phys. Rev. Lett. **103**, 087002 (2009).
[23] M.-H. Julien, H. Mayaffre, M. Horvatic, C. Berthier, X. D. Zhang, W. Wu, G. F. Chen, N. L. Wang, and J. L. Luo, EuroPhys. Lett. **87**, 37001 (2009).
[24] H. Chen, Y. Ren, Y. Qiu, Wei Bao, R. H. Liu, G. Wu, T. Wu, Y. L. Xie, X. F. Wang, Q. Huang and X. H. Chen, EuroPhys. Lett. **85**, 17006 (2009).
[25] Y. Zhang, J. Wei, H. W. Ou, J. F. Zhao, B. Zhou, F. Chen, M. Xu, C. He, G. Wu, H. Chen, M. Arita, K. Shimada, H. Namatame, M. Taniguchi, X. H. Chen, and D. L. Feng, Phys. Rev. Lett. **102**, 127003 (2009).
[26] R. H. Liu, G. Wu, T. Wu, D. F. Fang, H. Chen, S. Y. Li, K. Liu, Y. L. Xie, X. F. Wang, R. L. Yang, L. Ding, C. He, D. L. Feng, and X. H. Chen, Phys. Rev. Lett. **101**, 087001 (2008); A. J. Drew, Ch. Niedermayer, P. J. Baker, F. L. Pratt, S. J. Blundell, T. Lancaster, R. H. Liu, G.Wu, X. H. Chen, I.Watanabe, V. K. Malik, A. Dubroka, M. Rossle, K.W. Kim, C. Baines, and C. Bernhard, Nature mater. **8**, 310 (2009).
[27] K. Terashima, Y. Sekiba, J. H. Bowen, K. Nakayama, T. Kawahara, T. Sato, P. Richard, Y.-M. Xu, L. J. Li, G. H. Cao, Z.-A. Xu, H. Ding, and T. Takahashi, Proc. Natl. Acad. Sci. U.S.A. **106**, 7330 (2009); Y. Sekiba, T. Sato, K. Nakayama, K. Terashima, P. Richard, J. H. Bowen, H. Ding, Y.-M. Xu, L. J. Li, G. H. Cao, Z.-A. Xu, and T. Takahashi, New J. Phys. **11**, 025020 (2009).
[28] S. H. Pan and A. Li, private communication.
[29] Yi Gao, Tao Zhou, C. S. Ting, and Wu-Pei Su, Phys. Rev. B **82**, 104520 (2010).
[30] Yi Gao, Huai-Xiang Huang, Chun Chen, C. S. Ting, and Wu-Pei Su, Phys. Rev. Lett. **106**, 027004 (2011).
[31] H. M. Jiang, J.-X. Li, and Z. D. Wang, Phys. Rev. B **80**, 134505 (2009).
[32] A. M. Oles, G. Khaliullin, P. Horsch, and L. F. Feiner, Phys. Rev. B **72**, 214431 (2005).
[33] H. Ding, P. Richard, K. Nakayama, K. Sugawara, T. Arakane, Y. Sekiba, A. Takayama, S. Souma, T. Sato, T. Takahashi, Z. Wang, X. Dai, Z. Fang, G. F. Chen, J. L. Luo and N. L. Wang, Europhys. Lett. **83**, 47001 (2008).
[34] I. I. Mazin, D. J. Singh, M. D. Johannes, and M. H. Du, Phys. Rev. Lett. **101**, 057003 (2008).
[35] Kazuhiko Kuroki, Seiichiro Onari, Ryotaro Arita, Hidetomo Usui, Yukio Tanaka, Hiroshi Kontani, and Hideo Aoki, Phys.Rev.Lett. **101**, 087004 (2008).
[36] Fa Wang, Hui Zhai, Ying Ran, Ashvin Vishwanath, and Dung-Hai Lee, Phys. Rev. Lett. **102**, 047005 (2009).
[37] Zi-Jian Yao, Jian-Xin Li, and Z. D. Wang, New J. Phys. **11**, 025009 (2009).
[38] Y. Ran, F. Wang, H. Zhai, A. Vishwanath, and D.-H. Lee, Phys. Rev. B **79**, 014505 (2009).
[39] K. K. Huynh, Y. Tanabe, and K. Tanigaki, arXiv:1012.3029.
[40] Qiang Han and Z. D. Wang, New. J. Phys **11**, 025022 (2009).
[41] Clarina de la Cruz, Q. Huang, J. W. Lynn, Jiying Li, W. Ratcliff II, J. L. Zarestky, H. A. Mook, G. F. Chen, J. L. Luo, N. L. Wang, and Pengcheng Dai, Nature (London) **453**, 899 (2008).
[42] T.-M. Chuang, M. P. Allan, Jinho Lee, Yang Xie, Ni Ni, S. L. Bud'ko, G. S. Boebinger, P. C. Canfield, J. C. Davis, Science **327**, 181 (2010).
[43] Wei-Feng Tsai, Yan-Yang Zhang, Chen Fang, and Jiangping Hu, Phys. Rev. B **80**, 064513 (2009).
[44] T. O. Wehling, A. V. Balatsky, M. I. Katsnelson, A. I. Lichtenstein, K. Scharnberg, and R. Wiesendanger, Phys. Rev. B **75**, 125425 (2007).